IEICE TRANS. COMMUN., VOL.E106–B, NO.10 OCTOBER 2023

PAPER

Theoretical Analysis of Fully Wireless-Power-Transfer Node Networks

Hiroshi SAITO[†*a)], ***Fellow***

SUMMARY The performance of a fully wireless-power-transfer (WPT) node network, in which each node transfers (and receives) energy through a wireless channel when it has sufficient (and insufficient) energy in its battery, was theoretically analyzed. The lost job ratio (LJR), namely, is the ratio of (i) the amount of jobs that cannot be done due to battery of a node running out to (ii) the amount of jobs that should be done, is used as a performance metric. It describes the effect of the battery of each node running out and how much additional energy is needed. Although it is known that WPT can reduce the probability of the battery running out among a few nodes within a small area, the performance of a fully WPT network has not been clarified. By using stochastic geometry and first-passage-time analysis for a diffusion process, the expected LJR was theoretically derived. Numerical examples demonstrate that the key parameters determining the performance of the network are node density, threshold switching of statuses between "transferring energy" and "receiving energy," and the parameters of power conversion. They also demonstrate the followings: (1) The mean energy stored in the node battery decreases in the networks because of the loss caused by WPT, and a fully WPT network cannot decrease the probability of the battery running out under the current WPT efficiency. (2) When the saturation value of power conversion increases, a fully WPT network can decrease the probability of the battery running out although the mean energy stored in the node battery still decreases in the networks. This result is explained by the fact that the variance of stored energy in each node battery becomes smaller due to transfer of energy from nodes of sufficient energy to nodes of insufficient energy.

key words: *wireless power transfer (WPT), performance evaluation, stochastic geometry, first passage time, lost job ratio, probability of battery running out*

1. Introduction

Recently, the number of mobile devices in our environment has been rapidly growing. Millions of such devices require power via a battery, which must be frequently replaced. However, as the number of devices increases, such frequent large-scale replacement of batteries becomes infeasible. In the meantime, the number of wireless sensors installed in our environment is also increasing, and bundles of cables for supplying power to those sensors may become problematic. "Wireless power transfer" (WPT) is a promising technology for solving these problems [1], [2]. WPT is also essential for connecting a huge number of devices to the Internet of Things (IoT) [3].

Manuscript received December 12, 2022.
Manuscript revised February 18, 2023.
Manuscript publicized May 10, 2023.

[†]The author is with Graduate School of Information Science and Technology, the University of Tokyo, Tokyo, 113-8565 Japan.
[*]Presently, with Jissen Women's University, Tokyo, 191-8510 Japan.
a) E-mail: saito-hiroshi@jissen.ac.jp

DOI: 10.1587/transcom.2022EBP3204

Methods for implementing WPT include electromagnetic radiation, resonant coupling, capacitive coupling, and inductive coupling [4]. Among these methods, electromagnetic radiation uses electromagnetic waves such as radio-frequency waves as a medium to deliver energy in a form of radiation, and it can transfer energy over longer distances than other methods. In particular, its transfer range is more than several meters [4]. Some commercial products using electromagnetic radiation have already appeared [1], [5]. (Due to health concern, the number of Federal Communication Commission approvals for far field WPT has been limited [5].)

WPT energy sources can be classified as "dedicated" or "ambient", and each of those classifications can be sub-classified as "fixed" or "mobile." Dedicated sources are controllable, and deployed at known locations (fixed sources) or move along known routes (mobile sources). Their typical examples are power beacons (fixed sources) [6], [7] and mobile chargers (mobile sources) [8]. Energy transferred from dedicated sources is normally predictable. Determining locations of fixed sources or routes of mobile sources is often a research target [1] (and its references), [9]–[14]. Ambient sources such as wireless sensors with random transmissions (fixed or mobile sources) and vehicles connected to networks (mobile sources) often randomly fluctuate and their behavior is normally unpredictable. However, some ambient sources such as TV towers are predictable.

WPT nodes can be classified according to whether they are dedicated to charging (transferring energy) to other nodes and do not receive energy from other nodes or they can both transfer and receive energy. The latter is often called "relay nodes." The former is sub-classified into "fixed nodes" or "mobile nodes." A typical example of fixed dedicated chargers is a power beacon or a base station/access point with a charger function to charge mobile or wireless devices [6], [7], [10], [15]–[18]. That of mobile dedicated chargers is a mobile charger for working robots [8].

Examples of a relay node are a hybrid access point working as a relay to transfer energy to other nodes and transmit/receive information to/from nodes [19], [20] and a relay node for transmitting information between wireless devices and charging other nodes with insufficient energy through WPT in a multihop wireless network [21]. When relay nodes are introduced, spatial diversity increases and coverage widens. Existing studies on relay nodes have focused on optimization of parameters such as relay-node density [22] and power-splitting and time-switching ratios [23],

performance of protocols [19], and performance of relay systems such as the outage probability [24], [25]. For many other studies on relaying wireless power, see the references in [25].

Although WPT has been widely studied and it is known that a relay node using WPT can reduce the probability of running out of battery of a few nodes around it within a small area, the performance of networks fully implementing WPT has not been clarified yet. Accordingly, in this study, the performance of a wireless-node network in which every node, which may be a sensor node or a communication node, can transfer and receive wireless power was theoretically investigated. Hereafter, such a network is called a "fully wireless power transfer node network." Each node transfers its energy to other nodes via radio frequency (RF) if it has sufficient energy. When the energy originates from other nodes, the node functions as a relay node. Multi-hop relaying is also possible. The node may have an energy source such as a solar panel or mains power.

Analyzing the "lost job ratio," which is a performance metric, can answer the following three questions: (i) how well the performance of a network consisting of such nodes performs, (ii) which parameters are key to improving the performance, and (iii) what is the effect of fully wireless power transfer on the network. Lost job ratio is the amount of jobs that cannot be done due to the battery running out to the amount of jobs that should be done. The job amount is measured by the amount of energy a job uses. It is assumed that nodes are distributed in a homogeneous Poisson point process, and the lost job ratio of a typical node for a non-linear direct current (DC) power conversion from RF power is analyzed. To understand the impact of the spatial property, the condition that there are no other nodes within a given radius around the typical node is set for the analysis.

The major contributions of this paper are as follows:

(1) By using stochastic geometry and first passage time analysis for a diffusion process, the performance of a fully wireless-power-transfer node network is theoretically analyzed in terms of the lost job ratio, which describes the impact of the battery of each node running out on the performance of the network.

(2) Key parameters that affect the performance of the network are clarified. They are node density, threshold switching of statuses between "transferring energy to other nodes" and "receiving energy from other nodes," and the parameters of a DC power conversion from RF power. The importance of increasing the saturation value of this power conversion to reduce the lost job ratio can be a significant reason for developing an efficient means of power conversion.

(3) Numerical examples demonstrate the followings. (i) The mean energy stored in the node battery in the networks decreases because of the loss caused by WPT, and a fully WPT network cannot decrease the probability of running out of battery under the current WPT efficiency. (ii) However, the probability of running out of battery for a fully WPT network with high node density can decrease when efficient RF-DC power conversion is achieved (in particular, power conversion efficiency is not easily saturated), regardless of the decrease of the mean energy stored in the node battery in the network. This is because the variance of stored energy in the battery of each node becomes smaller when energy is transferred from nodes with sufficient energy to nodes with insufficient energy.

2. System Model and Assumption

In this study, a network composed of a set of nodes capable of WPT was analyzed. The nodes are distributed in a homogeneous Poisson point process (HPPP) $\Phi \subset \mathbb{R}^2$ with intensity (node density) λ. To simplify the notation, Φ is also used as the set of nodes, and $\mathbf{x} \in \Phi$ is used as the identifier of a node at $\mathbf{x}$.

Let $b_{\mathbf{x}}(t) \geq 0$ be the battery level (the amount of energy stored in the battery) and $s_{\mathbf{x}}(t) \in \{0, 1\}$ be the status at t of a node at $\mathbf{x} \in \Phi$. If $b_{\mathbf{x}}(t)$ is higher than threshold θ_H, the node transfers energy through a wireless channel with transmission power P_T to other nodes. The status $s_{\mathbf{x}}(t)$ of the node at time t is one (that is, $s_{\mathbf{x}}(t) = 1$), which denotes "energy transferring," and the status when the node is not transferring energy is zero (that is, $s_{\mathbf{x}}(t) = 0$). Other nodes with status of zero receive the transferred energy and store it in their battery. If the battery level of a node with $s_{\mathbf{x}}(t) = 1$ becomes lower than threshold θ_L (where $\theta_L < \theta_H$), the node stops transferring energy, and its status switches to zero. Let $\Phi_i(t)$ be a set of nodes with status i at t: that is, $\Phi_i(t) \equiv \{\mathbf{x} \in \Phi | s_{\mathbf{x}}(t) = i\}$. The transitions of $s_{\mathbf{x}}(t)$ are defined below (Fig. 1):

$$s_{\mathbf{x}}(t) = \begin{cases} 1 & \text{if } b_{\mathbf{x}}(t) > \theta_H \text{ or if } s_{\mathbf{x}}(t-1) = 1, b_{\mathbf{x}}(t) \geq \theta_L, \\ 0 & \text{if } b_{\mathbf{x}}(t) < \theta_L \text{ or if } s_{\mathbf{x}}(t-1) = 0, b_{\mathbf{x}}(t) \leq \theta_H. \end{cases} \tag{1}$$

$b_{\mathbf{x}}(t)$ is defined at the beginning of time slot t, and $s_{\mathbf{x}}(t)$ is determined on the basis of $b_{\mathbf{x}}(t)$ (Fig. 2). The transitions of $b_{\mathbf{x}}(t)$ are defined as

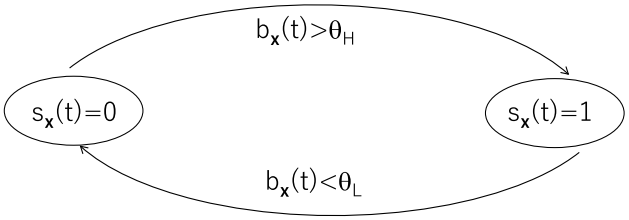

Fig. 1 Transition of $s_{\mathbf{x}}(t)$.

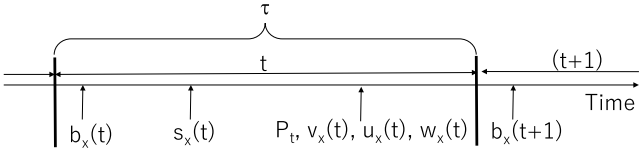

Fig. 2 Time slot.

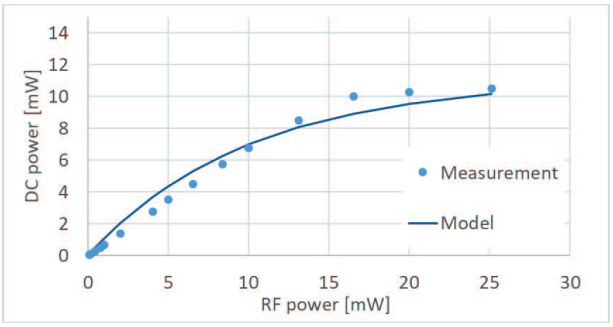

Fig. 3 RF power vs. DC power. Model is given by Eq. (4) with $\gamma_{sat} = \gamma_0 = 11.05$ and $\beta = 0.1$. Measurement data are regenerated from Fig. 8 in [3].

$$b_{\mathbf{x}}(t+1) = [b_{\mathbf{x}}(t)+\tau(u_{\mathbf{x}}(t)-P_T\mathbf{1}(s_{\mathbf{x}}(t)=1)+v_{\mathbf{x}}(t)-w_{\mathbf{x}}(t))]^+ \tag{2}$$

where τ is the length of the time slot, $[x]^+ = \max(0, x)$, $\mathbf{1}(x)$ is an indicator function, and $\mathbf{1}(x) = \begin{cases} 1 & \text{if } x \text{ is true,} \\ 0 & \text{otherwise.} \end{cases}$ The third term on the right-hand side of Eq. (2) means power consumption when energy is transferred to other nodes through a wireless channel with transmission power P_T. The second term $u_{\mathbf{x}}(t)$ is the amount of energy transferred from other nodes and is given as

$$u_{\mathbf{x}}(t) = \psi\Big(\sum_{\mathbf{y}\neq\mathbf{x}\in\Phi_1(t)} \frac{P_T G H_{\mathbf{x},\mathbf{y}}}{|\mathbf{x}-\mathbf{y}|^{\alpha}}\Big)\mathbf{1}(s_{\mathbf{x}}(t)=0), \tag{3}$$

where $\psi(\cdot) \geq 0$ is DC power converted from RF power, $\alpha > 2$ is a path-loss exponent, G is a constant gain, and $H_{\mathbf{x},\mathbf{y}}$ is small-scale fading (an independent random variable) modeled as Rayleigh fading with mean 1. On the basis of field data [26], [27], a few DC-to-RF power conversion models have been proposed [3], [28]–[32]. Among them, the model (Eq. (4)) proposed in [32] is used in the analysis of this paper because it is tractable with stochastic geometry.

$$\psi(x) = \gamma_{sat} - \gamma_0 \exp(-\beta x) \tag{4}$$

where γ_{sat}, γ_0, and β are constants determined by field data (Fig. 3). Although Eq. (4) is used for simplicity, it is possible to generalize the model to fit the field data better as follows:

$$\psi(x) = \gamma_{sat} - \sum_{k=1}^{K} \gamma_k \exp(-\beta_k x). \tag{5}$$

The extension to the analysis using this generalized model is straightforward.

When $s_{\mathbf{x}}(t) = 0$, a node can receive energy transferred from nodes in $\Phi_1(t)$ and store it in its battery. In addition, $v_{\mathbf{x}}(\cdot)$ is a random variable denoting energy supply from outside $\Phi_1(t)$ such as solar power supply, and $w_{\mathbf{x}}(\cdot)$ is also a random variable denoting miscellaneous energy consumption such as energy consumption for sensing rather than energy transfer. $\{v_{\mathbf{x}}(t)\}_{\mathbf{x},t}$ ($\{w_{\mathbf{x}}(t)\}_{\mathbf{x},t}$) are independent and identically distributed with mean $a_v \equiv E[v_{\mathbf{x}}(t)]$ ($a_w \equiv E[w_{\mathbf{x}}(t)]$) and variance $\sigma_v^2 \equiv var[v_{\mathbf{x}}(t)]$ ($\sigma_w^2 \equiv var[w_{\mathbf{x}}(t)]$). For stability of $b_{\mathbf{x}}(t)$, (i.e., $\lim_{t\to\infty} E[b_{\mathbf{x}}(t)] < \infty$), $P_T + a_w > a_v$ must be satisfied.

A list of notations is provided in Table 1.

Table 1 List of notations.

$[x]^+$	$[x]^+ = \max(0, x)$.
$B(r_b)$, $B(r_b)^c$	disk with center $\mathbf{o}$ and radius r_b, and its complement.
$\mathbf{1}(x)$	$\mathbf{1}(x) = \begin{cases} 1 & \text{if } x \text{ is true,} \\ 0 & \text{otherwise.} \end{cases}$
Φ	a set of locations of nodes
$\Phi_i(t)$	a set of locations of nodes with status i.
λ	intensity (node density) of Φ.
τ	time-slot length.
$b_{\mathbf{x}}(t)$	battery level at t of a node at $\mathbf{x} \in \Phi$.
$s_{\mathbf{x}}(t)$	status at t of a node at $\mathbf{x} \in \Phi$.
$u_{\mathbf{x}}(t)$	energy transferred from other nodes.
$v_{\mathbf{x}}(t)$, a_v	energy supply from outside $\Phi_1(t)$, $a_v \equiv E[v_{\mathbf{x}}(t)]$.
$w_{\mathbf{x}}(t)$, a_w	miscellaneous energy consumption, $a_w \equiv E[w_{\mathbf{x}}(t)]$.
σ_v^2, σ_w^2	$\sigma_v^2 \equiv var[v_{\mathbf{x}}(t)]$, $\sigma_w^2 \equiv var[w_{\mathbf{x}}(t)]$.
P_T	transmission power.
$\psi(\cdot)$	DC power converted from RF power.
α	path-loss exponent.
$H_{\mathbf{x},\mathbf{y}}$	small-scale fading (Rayleigh fading).
θ_H, θ_L	thresholds denoting start and stop of energy transfer.
q, $q_{\mathbf{o}}$	prob. of $s_{\mathbf{x}}(t) = 1$, conditional prob. of $s_{\mathbf{o}}(t) = 1$.
$\Phi^{\mathbf{o}}_{r_b}$	$\Phi \cap B(r_b)/\mathbf{o}$.
$A_k(\lambda, q, r_b)$	$\exp(-2\pi\lambda q \int_{r_b}^{\infty}(1 - \frac{1}{1+k\beta P_T G r^{-\alpha}})r\,dr)$.
$\eta(r)$	$\gamma_{sat} - \gamma_0 A_1(\lambda, q, r)$.
F_{LH}, F_{HL}	first passage times from θ_L to θ_H and from θ_H to θ_L.
a_{LH}, $\tilde{a}_{LH}$	$\tau(\eta(0) + a_v - a_w)$, $\tau(\eta(r_b) + a_v - a_w)$.
σ_{LH}	$\tau\sqrt{\sigma^2[u_{\mathbf{x}}(t)\|s_{\mathbf{x}}(t)=0] + \sigma_v^2 + \sigma_w^2}$.
$\tilde{\sigma}_{LH}$	$\tau\sqrt{\sigma_t^2[u_{\mathbf{o}}(t)\|\Phi^{\mathbf{o}}_{r_b} = \emptyset, s_{\mathbf{o}}(t)=0] + \sigma_v^2 + \sigma_w^2}$.

3. Analysis of Battery Level and Performance Metrics

The battery level $b_{\mathbf{o}}(t)$ of a typical node is theoretically analyzed hereafter in terms of "lost job ratio" (LJR) of the typical node. LJR is equivalent to the ratio of (i) the amount of energy a node wants to use but is not able to use due to its battery running out to (ii) the amount of energy a node wants to use. Accordingly, LJR is used to describe how much additional energy is needed.

It is assumed that a typical node is located at origin $\mathbf{o}$. According to Slivnyak's theorem [33], [34], the locations of nodes still follow an HPPP Φ under this assumption. The battery level and status of each node at t depend on the location of the node and the locations of other nodes. These spatio-temporal correlations highly complicate the analysis. This necessitates introducing the independent assumption that: *battery level and status of a node are independent of those of other nodes.* (A similar assumption was introduced in [35].) Under this assumption, $\Phi_1(t)$ is the thinned process of Φ with a Bernoulli thinning probability $q \equiv \Pr(s_{\mathbf{x}}(t) = 1)$. (For a point process Φ, the thinned process of Φ with a Bernoulli thinning probability q is a point process generated by independently removing each point in Φ with probability $1 - q$ and retaining it with probability q. If Φ is an HPPP with intensity λ, the thinned process becomes an HPPP with

intensity $q\lambda$.) Thus, the intensity of $\Phi_1(t)$ is λq. q is not depend on $\mathbf{x} \neq \mathbf{o}$.

The analysis of the performance of the typical node in a fully wireless-power-transfer node network is outlined as follows: (i) derive the first two moments of $u_{\mathbf{o}}(t), u_{\mathbf{x}}(t)$ as a function of q and $q_{\mathbf{o}} \equiv E[s_{\mathbf{o}}(t)|\Phi^{\mathbf{o}}_{r_b} = \emptyset] = \Pr(s_{\mathbf{o}}(t) = 1|\Phi^{\mathbf{o}}_{r_b} = \emptyset)$, which is the conditional average ratio of $s_{\mathbf{o}}(t) = 1$; (ii) obtain the expected first passage time $E[F_{LH}]$ ($E[F_{HL}]$) of $b_{\mathbf{o}}$ and that of $b_{\mathbf{x}}$ from θ_L to θ_H (from θ_H to θ_L) as a function of $q, q_{\mathbf{o}}$ on the basis of the first two moments $u_{\mathbf{o}}(t), u_{\mathbf{x}}(t)$ obtained in (i); (iii) describe q by using $E[F_{LH}(b_{\mathbf{x}})]$ and $E[F_{HL}(b_{\mathbf{x}})]$ with the renewal process theory, obtain a nonlinear equation of q using (ii), and solve it to get q; (iv) similarly, obtain $q_{\mathbf{o}}$ by using q, $E[F_{LH}(b_{\mathbf{o}})]$ and $E[F_{HL}(b_{\mathbf{o}})]$ by using (i)–(iii); and (v) obtain $E[LJR]$ by using q and $q_{\mathbf{o}}$.

To determine the impact of the spatial properties on the performance, we introduce r_b and evaluate the probabilities of $b_{\mathbf{o}}(t)$ and $s_{\mathbf{o}}(t)$ as well as $E[LJR]$ under the condition $\Phi^{\mathbf{o}}_{r_b} = \emptyset$, where $\Phi^{\mathbf{o}}_{r_b} \equiv \Phi \cap B(r_b)/\mathbf{o}$, which means $\Phi \cap B(r_b)$ excluding $\mathbf{o}$, and $B(r_b)$ is a disk with its center at $\mathbf{o}$ and the radius of r_b. This condition means that no nodes except for the typical node exist within r_b from the typical node. A large r_b corresponds to the case that there are no nodes near the typical node. Conversely, a small r_b corresponds to the case that there can be nodes near the typical node. The conditional probabilities become unconditional when $r_b = 0$.

3.1 Deriving First Two Moments of $u_{\mathbf{o}}(t), u_{\mathbf{x}}(t)$

To analyze $b_{\mathbf{o}}(t)$, the first conditional moment of $u_{\mathbf{o}}(t)$, namely, the conditional expectation of the amount of energy transferred from other nodes, is analyzed.

$$
\begin{aligned}
&E[u_{\mathbf{o}}(t)|\Phi^{\mathbf{o}}_{r_b} = \emptyset, s_{\mathbf{o}}(t) = 0] \\
&= E[\psi(\sum_{\mathbf{x}\neq\mathbf{o}\in\Phi_1(t)} \frac{P_T G H_{\mathbf{o},\mathbf{x}}}{|\mathbf{x}|^\alpha})|\Phi^{\mathbf{o}}_{r_b} = \emptyset] \\
&= \gamma_{sat} - \gamma_0 E[\prod_{\mathbf{x}\in\Phi_1(t)\cap B(r_b)^c} \exp(-\frac{\beta P_T G H_{\mathbf{o},\mathbf{x}}}{|\mathbf{x}|^\alpha})] \\
&\overset{(a)}{=} \gamma_{sat} \\
&\quad -\gamma_0 E[\prod_{\mathbf{x}\in\Phi\cap B(r_b)^c} (1 - q + q\exp(-\frac{\beta P_T G H_{\mathbf{o},\mathbf{x}}}{|\mathbf{x}|^\alpha}))] \\
&\overset{(b)}{=} \gamma_{sat} - \gamma_0 E[\prod_{\mathbf{x}\in\Phi\cap B(r_b)^c} (1 - q + \frac{q}{1 + \beta P_T G|\mathbf{x}|^{-\alpha}})] \\
&\overset{(c)}{=} \gamma_{sat} - \gamma_0 \exp(-\lambda \int_{B(r_b)^c} (q - \frac{q}{1 + \beta P_T G|\mathbf{x}|^{-\alpha}}) d\mathbf{x}) \\
&= \eta(r_b), \qquad (6)
\end{aligned}
$$

where $\eta(r_b) \equiv \gamma_{sat} - \gamma_0 A_1(\lambda, q, r_b)$, $A_k(\lambda, q, r_b) \equiv \exp(-2\pi\lambda q \int_{r_b}^{\infty} (1 - \frac{1}{1+k\beta P_T G r^{-\alpha}}) r\, dr)$. (a) is because $\Phi_1(t)$ is the thinned process of Φ with thinning probability q, and $\mathbf{x} \in \Phi(t)$ is not included in $\Phi_1(t)$ with prob. $1 - q$ but is included with prob. q. (b) is because $H_{\mathbf{o},\mathbf{x}}$ follows exp(1). Thus, $\int e^{-s\omega} H_{\mathbf{o},\mathbf{x}}(\omega) d\omega = 1/(1 + s)$. (c) is due to the moment generating functional (MGF) for an HPPP. The MGF for an HPPP $\{\mathbf{x}_i\}_i$ of intensity ρ in Ω is given as follows [34]. For a generic function $h(\mathbf{x})$,

$$
E[\prod_i h(\mathbf{x}_i)] = \exp(-\rho \int_\Omega (1 - h(\mathbf{x})) d\mathbf{x}). \qquad (7)
$$

Therefore,

$$
E[u_{\mathbf{o}}(t)|\Phi^{\mathbf{o}}_{r_b} = \emptyset, s_{\mathbf{o}}(t) = 0] = \eta(r_b), \qquad (8)
$$

$$
E[u_{\mathbf{o}}(t)|\Phi^{\mathbf{o}}_{r_b} = \emptyset] = \eta(r_b)(1 - q_{\mathbf{o}}). \qquad (9)
$$

Similarly, $E[u_{\mathbf{o}}(t)^2|\Phi^{\mathbf{o}}_{r_b} = \emptyset, s_{\mathbf{o}}(t) = 0]$ can be obtained as follows.

$$
\begin{aligned}
&E[u_{\mathbf{o}}(t)^2|\Phi^{\mathbf{o}}_{r_b} = \emptyset, s_{\mathbf{o}}(t) = 0] \\
&= E[\psi(\sum_{\mathbf{x}\neq\mathbf{o}\in\Phi_1(t)} \frac{P_T G H_{\mathbf{o},\mathbf{x}}}{|\mathbf{x}|^\alpha})^2|\Phi^{\mathbf{o}}_{r_b} = \emptyset] \\
&= \gamma_{sat}^2 - 2\gamma_{sat}\gamma_0 E[\prod_{\mathbf{x}\in\Phi_1(t)\cap B(r_b)^c} \exp(-\frac{\beta P_T G H_{\mathbf{o},\mathbf{x}}}{|\mathbf{x}|^\alpha})] \\
&\quad +\gamma_0^2 E[\prod_{\mathbf{x}\in\Phi_1(t)\cap B(r_b)^c} \exp(-\frac{2\beta P_T G H_{\mathbf{o},\mathbf{x}}}{|\mathbf{x}|^\alpha})] \\
&= \gamma_{sat}^2 - 2\gamma_{sat}\gamma_0 A_1(\lambda, q, r_b) + \gamma_0^2 A_2(\lambda, q, r_b). \qquad (10)
\end{aligned}
$$

Thus,

$$
\begin{aligned}
&\sigma_t^2[u_{\mathbf{o}}(t)|\Phi^{\mathbf{o}}_{r_b} = \emptyset, s_{\mathbf{o}}(t) = 0] \\
&\equiv E[u_{\mathbf{o}}(t)^2|\Phi^{\mathbf{o}}_{r_b} = \emptyset, s_{\mathbf{o}}(t) = 0] \\
&\qquad -E^2[u_{\mathbf{o}}(t)|\Phi^{\mathbf{o}}_{r_b} = \emptyset, s_{\mathbf{o}}(t) = 0] \\
&= \gamma_0^2(A_2(\lambda, q, r_b) - A_1(\lambda, q, r_b)^2). \qquad (11)
\end{aligned}
$$

Similarly to Eqs. (8), (10) and (11),

$$
E[u_{\mathbf{x}}(t)|s_{\mathbf{x}}(t) = 0] = \eta(0), \qquad (12)
$$

$$
\begin{aligned}
&E[u_{\mathbf{x}}(t)^2|s_{\mathbf{x}}(t) = 0] \\
&= (\gamma_{sat}^2 - 2\gamma_{sat}\gamma_0 A_1(\lambda, q, 0) + \gamma_0^2 A_2(\lambda, q, 0)), \qquad (13)
\end{aligned}
$$

$$
\sigma^2[u_{\mathbf{x}}(t)|s_{\mathbf{x}}(t) = 0] = \gamma_0^2(A_2(\lambda, q, 0) - A_1(\lambda, q, 0)^2). \qquad (14)
$$

3.2 Obtaining First Passage Time of $b_{\mathbf{x}}$

The first passage times $F_{LH}(b_{\mathbf{x}})$ and $F_{HL}(b_{\mathbf{x}})$ of $b_{\mathbf{x}}$ from θ_L to θ_H and from θ_H to θ_L are defined as follows (Fig. 4):

$$
F_{LH}(b_{\mathbf{x}}) = \inf(t > 0; b_{\mathbf{x}}(s) = \theta_L, b_{\mathbf{x}}(s + t) \geq \theta_H) \qquad (15)
$$

$$
F_{HL}(b_{\mathbf{x}}) = \inf(t > 0; b_{\mathbf{x}}(s) = \theta_H, b_{\mathbf{x}}(s + t) \leq \theta_L). \qquad (16)
$$

Equation (2), which describes the battery level behavior, is quite similar to a queue of packets. Therefore, the diffusion process approximation, which is commonly used in queuing theory, is used for analyzing the first passage times of battery level.

Because $s_{\mathbf{x}} = 1$ during the passage time from θ_H to θ_L, $b_{\mathbf{x}}(\cdot)$ is approximated by a Brownian motion (the simplest diffusion approximation) with drift $E[\tau(-P_T + v_{\mathbf{x}}(t) - w_{\mathbf{x}}(t))]$ during the passage from θ_H to θ_L. According to [36], the first moment of $F_{HL}(b_{\mathbf{x}})$ is given as follows.

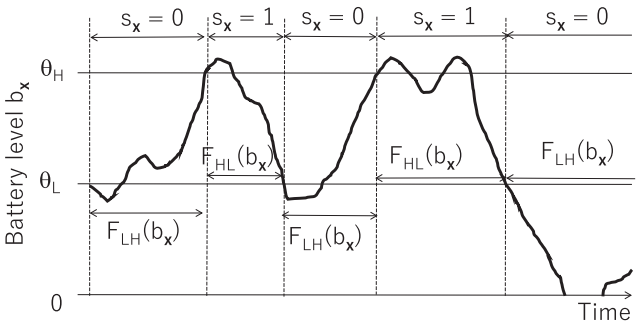

Fig. 4 Illustration of first passage time.

$$E[F_{HL}](b_{\mathbf{x}}) = (\theta_H - \theta_L)/(\tau E[P_T - v_{\mathbf{x}}(t) + w_{\mathbf{x}}(t)]) = (\theta_H - \theta_L)/(\tau(P_T - a_v + a_w)) \quad (17)$$

Note that $s_{\mathbf{x}} = 0$ during the passage time from θ_L to θ_H. Therefore, $b_{\mathbf{x}}(\cdot)$ is approximated as a diffusion process with a reflecting barrier at zero, an absorbing barrier at θ_H, drift $a_{LH} \equiv \tau(\eta(0) + a_v - a_w)$, and diffusion $\sigma_{LH} \equiv \tau\sqrt{\sigma^2[u_{\mathbf{x}}(t)|s_{\mathbf{x}}(t) = 0] + \sigma_v^2 + \sigma_w^2}$ during its passage from θ_L to θ_H, where $\sigma^2[u_{\mathbf{x}}(t)|s_{\mathbf{x}}(t) = 0]$ is given by Eq. (14). Applying Case D on page 1010 in [37] or Eq. (2.15) in [38] to $E[F_{LH}(b_{\mathbf{x}})]$ gives

$$\begin{aligned} &E[F_{LH}(b_{\mathbf{x}})] \\ &= \frac{\theta_H - \theta_L}{\tau(\eta(0) + a_v - a_w)} \\ &\quad - \frac{\sigma^2[u_{\mathbf{x}}(t)|s_{\mathbf{x}}(t) = 0] + \sigma_v^2 + \sigma_w^2}{2(\eta(0) + a_v - a_w)^2} \\ &\quad \{\exp(-\frac{2(\eta(0) + a_v - a_w)\theta_L}{\tau(\sigma^2[u_{\mathbf{x}}(t)|s_{\mathbf{x}}(t) = 0] + \sigma_v^2 + \sigma_w^2)}) \\ &\quad - \exp(-\frac{2(\eta(0) + a_v - a_w)\theta_H}{\tau(\sigma^2[u_{\mathbf{x}}(t)|s_{\mathbf{x}}(t) = 0] + \sigma_v^2 + \sigma_w^2)})\}. \\ &= \frac{\theta_H - \theta_L}{a_{LH}} \\ &\quad - \frac{\sigma_{LH}^2}{2a_{LH}^2}\{\exp(-\frac{2a_{LH}\theta_L}{\sigma_{LH}^2}) - \exp(-\frac{2a_{LH}\theta_H}{\sigma_{LH}^2})\}. \end{aligned} \quad (18)$$

3.3 Obtaining q

Due to the renewal process theory applying to an alternating renewal process,

$$q = \Pr(s_{\mathbf{x}}(t) = 1) = E[F_{HL}(b_{\mathbf{x}})]/(E[F_{HL}(b_{\mathbf{x}})] + E[F_{LH}(b_{\mathbf{x}})]). \quad (19)$$

Therefore,

$$q(E[F_{HL}(b_{\mathbf{x}})] + E[F_{LH}(b_{\mathbf{x}})]) - E[F_{HL}(b_{\mathbf{x}})] = 0. \quad (20)$$

Note that $E[F_{LH}(b_{\mathbf{x}})]$ is a function of q. q (i.e., $\Pr(s_{\mathbf{x}}(t) = 1)$) is the solution of Eq. (20). The left-hand side of the equation becomes $-E[F_{HL}(b_{\mathbf{x}})] < 0$ for $q = 0$ and becomes $E[F_{HL}(b_{\mathbf{x}})] > 0$ for $q = 1$. Thus, Eq. (20) has a solution in $(0, 1)$. Solving it obtains q.

3.4 Obtaining First Passage Time of $b_{\mathbf{o}}$ and $q_{\mathbf{o}}$

Similar to the first passage times $F_{LH}(b_{\mathbf{x}})$ and $F_{HL}(b_{\mathbf{x}})$ of $b_{\mathbf{x}}$,

$$E[F_{HL}(b_{\mathbf{o}})] = (\theta_H - \theta_L)/(\tau(P_T - a_v + a_w)), \quad (21)$$

$$\begin{aligned} &E[F_{LH}(b_{\mathbf{o}})] \\ &= \frac{\theta_H - \theta_L}{\tau(\eta(r_b) + a_v - a_w)} \\ &\quad - \frac{\sigma_t^2[u_{\mathbf{o}}(t)|\Phi_{r_b}^{\mathbf{o}} = \emptyset, s_{\mathbf{o}}(t) = 0] + \sigma_v^2 + \sigma_w^2}{2(\eta(r_b) + a_v - a_w)^2} \\ &\quad \{\exp(-\frac{2(\eta(r_b) + a_v - a_w)\theta_L}{\tau(\sigma_t^2[u_{\mathbf{o}}(t)|\Phi_{r_b}^{\mathbf{o}} = \emptyset, s_{\mathbf{o}}(t) = 0] + \sigma_v^2 + \sigma_w^2)}) \\ &\quad - \exp(-\frac{2(\eta(r_b) + a_v - a_w)\theta_H}{\tau(\sigma_t^2[u_{\mathbf{o}}(t)|\Phi_{r_b}^{\mathbf{o}} = \emptyset, s_{\mathbf{o}}(t) = 0] + \sigma_v^2 + \sigma_w^2)})\}, \\ &= \frac{\theta_H - \theta_L}{\tilde{a}_{LH}} \\ &\quad - \frac{\tilde{\sigma}_{LH}^2}{2\tilde{a}_{LH}^2}\{\exp(-\frac{2\tilde{a}_{LH}\theta_L}{\tilde{\sigma}_{LH}^2}) - \exp(-\frac{2\tilde{a}_{LH}\theta_H}{\tilde{\sigma}_{LH}^2})\}. \end{aligned} \quad (22)$$

Here, $\tilde{a}_{LH} \equiv \tau(\eta(r_b) + a_v - a_w)$ and $\tilde{\sigma}_{LH} \equiv \tau\sqrt{\sigma_t^2[u_{\mathbf{o}}(t)|\Phi_{r_b}^{\mathbf{o}} = \emptyset, s_{\mathbf{o}}(t) = 0] + \sigma_v^2 + \sigma_w^2}$. Therefore, $q_{\mathbf{o}}$ satisfies

$$q_{\mathbf{o}}(E[F_{HL}(b_{\mathbf{o}})] + E[F_{LH}(b_{\mathbf{o}})]) - E[F_{HL}(b_{\mathbf{o}})] = 0. \quad (23)$$

Similar to Eq. (20), this equation has a solution in $(0, 1)$ because the left-hand side of this equation becomes $-E[F_{HL}(b_{\mathbf{o}})] < 0$ for $q_{\mathbf{o}} = 0$ and becomes $E[F_{HL}(b_{\mathbf{o}})] > 0$ for $q_{\mathbf{o}} = 1$. Solving it by using q obtains $q_{\mathbf{o}}$. (Note that $E[F_{LH}(b_{\mathbf{o}})]$ is a function of q because $\eta(r_b)$ is a function of q.)

3.5 Obtaining Lost Job Ratio

Since q and $q_{\mathbf{o}}$ were derived, the performance metric of interest, $E[LJR]$, of the typical node when no other nodes exist within r_b, can be obtained as follows. Note that the time average of the total energy consumed by the typical node including the transferred energy and energy used is $P_T q_{\mathbf{o}} + a_w$, and that of the energy offered is $E[u_{\mathbf{o}}(t)|\Phi_{r_b}^{\mathbf{o}} = \emptyset] + a_v = \eta(r_b)(1 - q_{\mathbf{o}}) + a_v$. If the former is larger than the latter, that is, if the typical node wants to use energy to do a job but necessary energy is larger than offered energy, the typical node must give up the job. This situation is referred to as "lost job", and the energy insufficiency causing lost job in average is $P_T q_{\mathbf{o}} + a_w - (\eta(r_b)(1 - q_{\mathbf{o}}) + a_v)$. (Because a long time average is considered, it is unnecessary to take account of stored energy at time 0 if it is finite.) Here, the amount of job is measured by the energy the job needs. Therefore, the amount of lost job is $P_T q_{\mathbf{o}} + a_w - (\eta(r_b)(1 - q_{\mathbf{o}}) + a_v)$ in average, and the amount of job the typical node wants to do is $P_T q_{\mathbf{o}} + a_w$.

Therefore, the lost job ratio in average is given as

$$E[LJR] = 1 - (\eta(r_b)(1 - q_{\mathbf{o}}) + a_v)/(P_T q_{\mathbf{o}} + a_w). \quad (24)$$

The lost job ratio describes how large additional energy is needed.

4. Numerical Examples

If not explicitly mentioned otherwise, the following conditions were used in the following numerical examples: $\lambda = 0.1$, $\alpha = 4$, $\gamma_{sat} = \gamma_0 = 11.05$, $\beta = 0.1$, $G = 1$, $P_T = 50$mW, $a_v = 10$mW, $\sigma_v = 100$mW, $a_w = 10$mW, $\sigma_w = 100$mW, $\theta_H = 100$, $\theta_L = 50$, and $\tau = 0.01$s. $v_{\mathbf{x}}$ and $w_{\mathbf{x}}$ follow normal distributions. The simulation is very time-consuming due to spatial-temporal randomness. In each simulation run, there were 5×10^4 time slots and the first 10^4 time slots were not used as an initial period to derive results. 200 simulation runs were conducted to determine each point of a graph.

$E[LJR]$ is plotted against λ in Fig. 5. As expected, $E[LJR]$ decreases as λ increases. This result can be explained by the fact that the number of nodes that can transfer energy increases as λ increases and the energy transferred from those nodes increases. For $r_b = 0$ (i.e., without conditions on nearby nodes), $E[LJR]$ is reduced about 80% when λ became five times larger. For larger r_b, the reduction of $E[LJR]$ is smaller. This result can be explained by the fact that nodes outside $B(r_b)$ were too far to sufficiently transfer a large amount of energy. That is, the typical node was almost isolated and could not benefit from the effect of the WPT node network for a large r_b.

In Fig. 5, as λ increases, the difference between $E[LJR]$ derived from Eq. (24) and that obtained by simulation becomes larger. The former was smaller than the latter. This seems to be because there was a small positive correlation between the status of the typical node and that of the nearest node, $\eta(r_b)$ under the assumption of independence became larger than the true $\eta(r_b)$ and resulted in a smaller $E[LJR]$ than the true $E[LJR]$. In addition, because $\eta(r_b)$ became larger as λ increased, and the influence of its error on $E[LJR]$ in Eq. (24) became clearer.

The impact of λ on $E[LJR]$ was non-linear. As λ increased, the energy transferred from other nodes increased because the number of surroundings nodes increased. This is the direct impact of λ. The nodes receiving such energy could therefore reach $s_{\mathbf{x}}(t) = 1$ (the status transferring energy) sooner. As a result, the ratio of nodes transferring energy to other nodes increased. This is the indirect impact of λ, which is demonstrated in Fig. 6 where $q_{\mathbf{o}} = \Pr(s_{\mathbf{o}} = 1 | \Phi^{\mathbf{o}}_{r_b} = \emptyset)$ plotted against λ increases as λ increases. The direct and indirect impacts causes super-linear impact, as shown in Figs. 5 and 6. However, for large r_b, this impact is very small, because the number of nodes transferring to the typical node is small and the energy received from them is small.

The energy transferred from other nodes to the typical node $\eta(r_b)(1 - q_{\mathbf{o}})$ and that transferred from the typical node to other nodes $P_T q_{\mathbf{o}}$ are plotted in Fig. 7. This figure demonstrates the following: (i) energy transferred from the typical node is larger than that transferred to the typical node (that is, WPT caused energy loss); (ii) as λ increases, the loss becomes smaller for any r_b (because λ has an upper limit due to physical factors such as antenna size, the total energy received cannot be larger than the energy transferred); (iii) for small r_b and large λ, the loss is small.

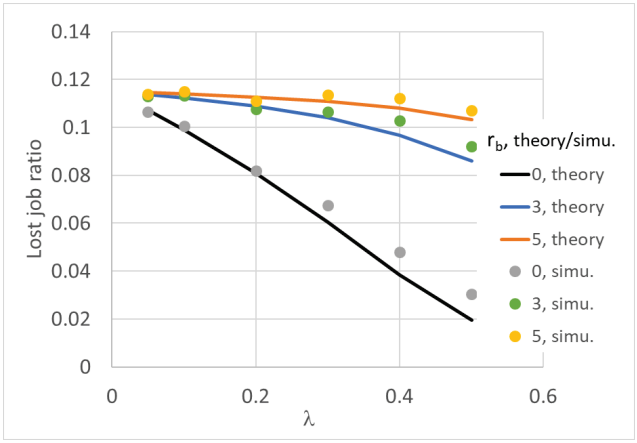

Fig. 5 $E[LJR]$ vs. λ with various r_b.

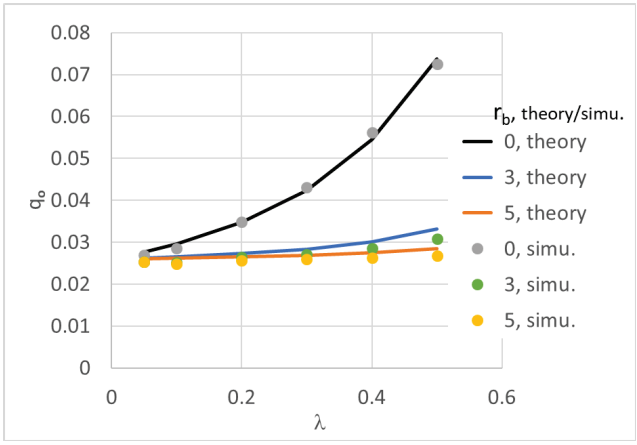

Fig. 6 $q_{\mathbf{o}}$ vs. λ with various r_b.

Because the amount of energy transfered to other nodes from a node transferring energy is P_T and is independent of the number of nodes receiving the transferred energy, the amount of energy received by a node and the number of nodes receiving energy increase as the number of nodes increases. The loss is thus smaller for larger λ. The energy transferred from the typical node increases as λ increases because of the increase of $\Pr(s_{\mathbf{o}} = 1 | \Phi^{\mathbf{o}}_{r_b} = \emptyset)$. For large r_b, the energy transferred from the other nodes to the typical node is small because there are no nodes near the typical node even when λ is large. The impact of λ is thus small for large r_b.

As shown in Fig. 7, energy transfer causes energy loss in the case WPT is applied. Actually, mean battery level in the case WPT is applied was lower than that in the case WPT is not applied ("Mean battery level" in Fig. 8). Thus, there is a concern that the probability of the battery running out increases by using WPT. To investigate this concern,

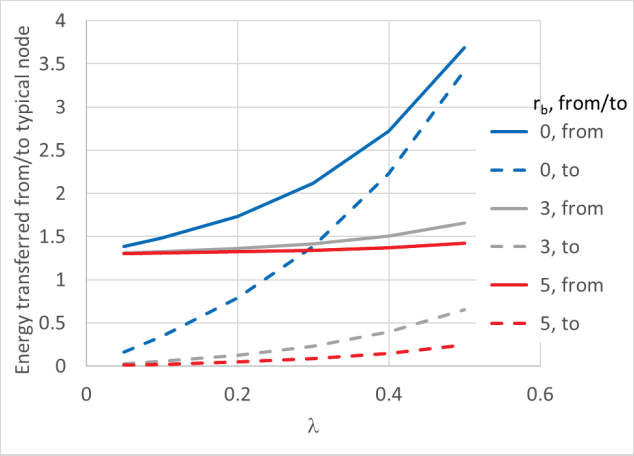

Fig. 7 Energy transferred to and from typical node vs. λ with various r_b.

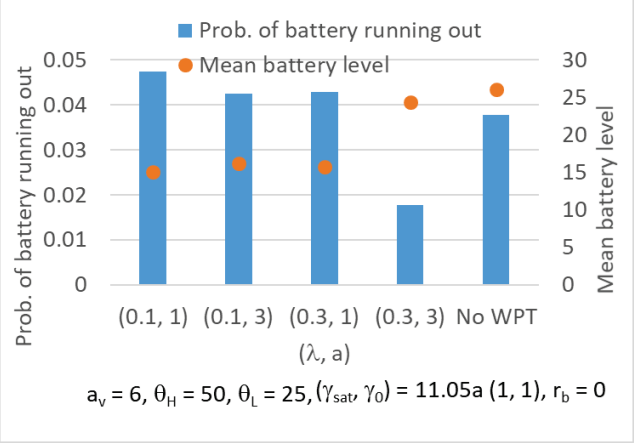

Fig. 8 $\Pr(b_{\mathbf{o}} = 0)$ and $E[b_{\mathbf{o}}]$ with and without WPT (simulation result).

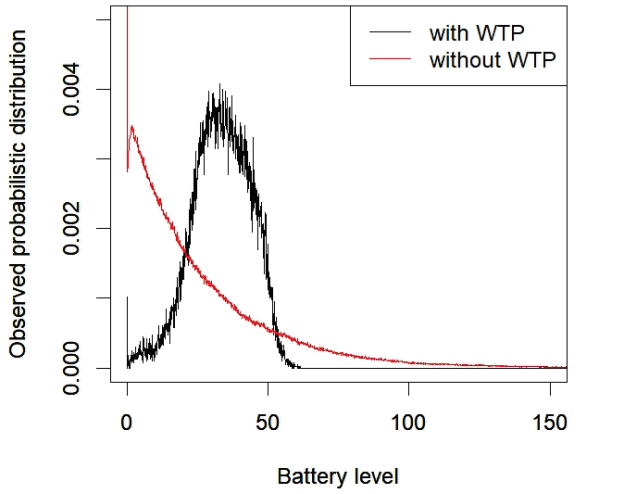

$\lambda = 0.3, \gamma_{sat} = \gamma_0 = 33.15, a_v = 6, \theta_H = 50, \theta_L = 25, r_b = 0$

Fig. 9 Observed $\Pr(b_{\mathbf{o}})$ with and without WPT (simulation result).

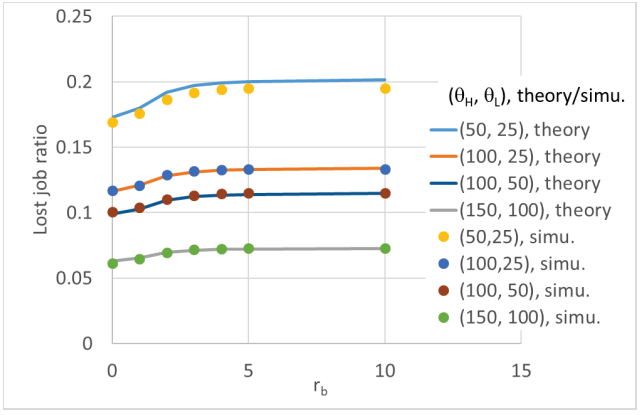

Fig. 10 Effect of θ_H and θ_L on $E[LJR]$.

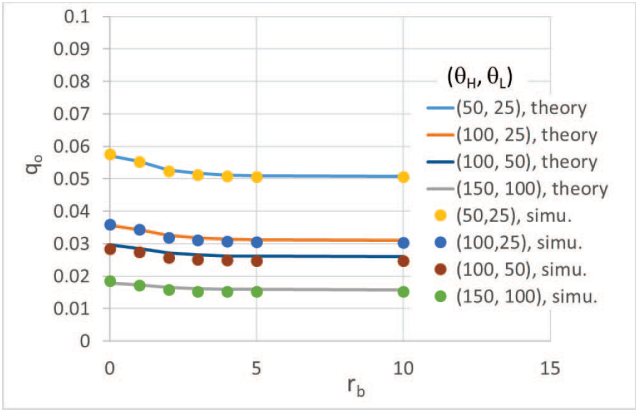

Fig. 11 Effect of θ_H and θ_L on $q_{\mathbf{o}}$.

the probability of the battery running out in the case WPT is applied was compared with that without WPT. (Note that, for stability of $b_{\mathbf{x}}(t)$ without WPT, $a_w > a_v$ must be satisfied. Therefore, $a_v = 6$ was used in Figs. 8 and 9.)

Figure 8 demonstrated that the probability of the battery running out, $\Pr(b_{\mathbf{o}} = 0)$, can decrease for fairly high node density and efficient RF-DC conversion, even when $E[b_{\mathbf{o}}]$ decreases. This result is due to the fact that the variance of stored energy in each node battery becomes smaller due to transferring energy from nodes of sufficient energy to nodes of insufficient energy by WPT. Figure 9 illustrates this fact. $\Pr(b_{\mathbf{o}} > \theta_H)$ becomes very small and $\Pr(\theta_L < b_{\mathbf{o}} < \theta_H)$ very large in the case WPT is applied, and $\Pr(b_{\mathbf{o}} > \theta_H)$ and $\Pr(b_{\mathbf{o}} < \theta_L)$ become very large in the case WPT is not applied. However, $\Pr(b_{\mathbf{o}} = 0)$ can increase even when WPT is applied if node density is low or RF-DC conversion is inefficient (Fig. 8).

In Fig. 10, $E[LJR]$ vs. r_b with various θ_H and θ_L is plotted. $E[LJR]$ increases as r_b increases for all combinations of θ_H and θ_L. This result is due to the fact that no nodes exist within r_b around the typical node and the number of nodes transferring energy to the typical node decreases as r_b increases. Because the number of nodes transferring energy to the typical node decreases as r_b increases and the energy transferred to the typical node decreases, $q_{\mathbf{o}}(= \Pr(s_{\mathbf{o}} = 1))$ decreases as r_b increases (Fig. 11).

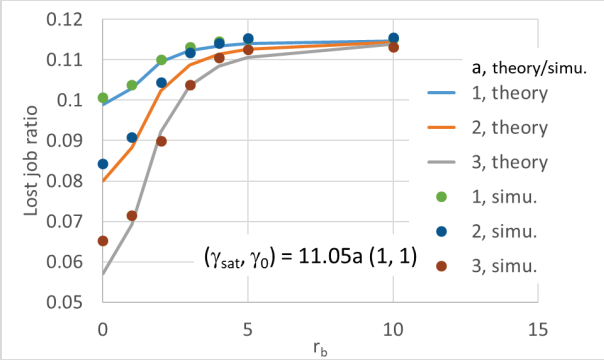

Fig. 12 Impact of non-linearity of power conversion with various a ($\gamma_{sat} = \gamma_0 = 11.05a$).

$E[LJR]$ and $q_{\mathbf{o}}$ are large when θ_H or θ_L is small. As θ_H or θ_L increases, $E[LJR]$ and $q_{\mathbf{o}}$ decreases (Figs. 10 and 11). The increase of $q_{\mathbf{o}}$ did not result in the increase of $E[LJR]$. This result seems to be due to the fact that the energy transfer causes energy loss (Fig. 7). Thus, the increase of $q_{\mathbf{o}}$ may not contribute to the decrease of $E[LJR]$. (When λ increases, the number of nodes increases in addition to the increase of $q_{\mathbf{o}}$. Hence, the increase of energy received from other nodes is larger than energy loss. Thus, the increase of $q_{\mathbf{o}}$ and the decrease of $E[LJR]$ are simultaneous. See Figs. 5 and 6.)

According to Fig. 11, $q_{\mathbf{o}}$ is large when θ_H or θ_L is small. Large θ_H means that a node rarely reaches the status $s_{\mathbf{x}}(t) = 1$ (i.e., the status for transferring energy to other nodes) and that the decrease of battery level at each time slot at that status is $P_T - a_v + a_w$ in average and is not dependent on θ_H or θ_L. Thus, large θ_H results in small $q_{\mathbf{o}}$. For fixed θ_H, small θ_L means that a node is likely to stay in the status $s_{\mathbf{x}}(t) = 1$ longer. Thus, small θ_L results in large $q_{\mathbf{o}}$.

The impact of the non-linearity of DC power conversion from RF power on $E[LJR]$ was investigated as follows. Under the assumption that $\gamma_{sat} = \gamma_0 = 11.05a$, $E[LJR]$ is plotted in Fig. 12, where a is a parameter denoting that saturation power becomes a times larger than that of the current conversion. For small r_b, a has a large impact. Particularly for $r_b = 0$, $E[LJR]$ decreased 20% smaller for $a = 2$ and 40% for $a = 3$. This result suggests the importance of developing an efficient conversion device for fully WPT node networks.

As a increases, the difference between the theoretically derived $E[LJR]$ and that obtained by simulation becomes larger. The former was smaller than the latter. The reason for this error seems to be the same as that for the error in Fig. 5.

5. Conclusion

The performance of a fully WPT node networks was investigated by using a theoretical method with stochastic geometry and first passage time analysis. As a performance metric, $E[LJR]$ was used, and an efficient method for computing it was developed.

Numerical examples clarified that λ, θ_H, θ_L, γ_{sat}, and γ_0 are key parameters determining performance. For large node density, appropriate θ_H and θ_L values, and efficient DC power conversion from RF power, $E[LJR]$ can be significantly improved. In particular, it was demonstrated that the development of efficient power conversion is important for implementing fully WPT node networks. However, a node located far away from other nodes cannot benefit from the effect of a wireless power transfer node network. A function for detecting such isolation may be needed in each node to overcome this problem.

Numerical examples demonstrated that mean stored energy in the network decreases because of energy loss caused by WPT and that a fully WPT network cannot decrease the probability of the battery running out. However, the probability of the battery running out decreases even under the decrease of the mean stored energy in the network when node density is high and DC power conversion from RF power is efficient. This result is explained by the fact that the variance of stored energy in each node battery becomes smaller due to energy transfer from nodes with sufficient energy to nodes with insufficient energy. It is therefore concluded that fully WPT node networks will benefit users by reducing the probability of the battery running out when efficient RF-DC power conversion is implemented.

An R program I developed for theoretically calculating the metrics such as $E[LJR]$ in this paper is available at [39]. Please refer to this paper for its use.

Acknowledgments

This work was supported by KAKENHI JSPS Grant Number JP-21K11864.

References

[1] X. Lu, P. Wang, D. Niyato, D.I. Kim, and Z. Han, "Wireless charging technologies: Fundamentals, standards, and network applications," IEEE Commun. Survey Tuts., vol.18, no.2, pp.1413–1452, 2016.
[2] H. Tabassum, E. Hossain, A. Ogundipe, and D.I. Kim, "Wireless-powered cellular networks: Key challenges and solution techniques," IEEE Commun. Mag., vol.53, no.6, pp.63–71, 2015.
[3] B. Clerckx, R. Zhang, R. Schober, D.W.K. Ng, D.I. Kim, and H.V. Poor, "Fundamentals of wireless information and power transfer: From RF energy harvester models to signal and system designs," IEEE J. Sel. Areas Commun., vol.37, no.1, pp.4–33, 2019.
[4] H. Shoki, "Wireless power transmission technologies to realize internet of energy society," IEICE J., vol.100, no.10, pp.1009–1015, 2020 (in Japanese).
[5] J. Huang, Y. Zhou, Z. Ning, and H. Gharavi, "Wireless power transfer and energy harvesting: Current status and future prospects," IEEE Wireless Commun., vol.26, no.4, pp.163–169, Aug. 2019.
[6] H. Tabassum and E. Hossain, "On the deployment of energy sources in wireless-powered cellular networks," IEEE Trans. Commun., vol.63, no.9, pp.3391–3404, 2015.
[7] K. Huang and V.K.N. Lau, "Enabling wireless power transfer in cellular networks: Architecture, modeling and deployment," IEEE Trans. Wireless Commun., vol.13, no.2, pp.902–912, 2014.
[8] L. He, P. Cheng, Y. Gu, J. Pan, T. Zhu, and C. Liu, "Mobile-to-mobile energy replenishment in mission-critical robotic sensor networks," IEEE INFOCOM 2014, 2014.

[9] H. Dai, Y. Liu, N. Yu, C. Wu, G. Chen, T. He, and A.X. Liu, "Radiation constrained wireless charger placement," IEEE/ACM Trans. Netw., vol.29, no.1, pp.48–64, 2021.
[10] Y. Li, Y. Chen, C.S. Chen, Z. Wang, and Y.-H. Zhu, "Charging while moving: Deploying wireless chargers for powering wearable devices," IEEE Trans. Veh. Technol., vol.67, no.12, pp.11575–11586, 2018.
[11] Y. Sun, C. Lin, H. Dai, P. Wang, L. Wang, G. Wu, and Q. Zhang, "Trading off charging and sensing for stochastic events monitoring in WRSNs," IEEE/ACM Trans. Netw., vol.30, no.2, pp.557–571, 2022.
[12] X. Wang, H. Dai, W. Wang, J. Zheng, N. Yu, G. Chen, W. Dou, and X. Wu, "Practical heterogeneous wireless charger placement with obstacles," IEEE Trans. Mobile Comput., vol.19, no.8, pp.1910–1927, 2020.
[13] T. Liu, B. Wu, S. Zhang, J. Peng, and W. Xu, "An effective multi-node charging scheme for wireless rechargeable sensor networks," IEEE INFOCOM 2020, 2020.
[14] W. Xu, W. Liang, X. Jia, H. Kan, Y. Xu, and X. Zhang, "Minimizing the maximum charging delay of multiple mobile chargers under the multi-node energy charging scheme," IEEE Trans. Mobile Comput., vol.20, no.5, pp.1846–1861, 2021.
[15] Q. Gu, Y. Jian, G. Wang, R. Fan, H. Jiang, and Z. Zhong, "Mobile edge computing via wireless power transfer over multiple fading blocks: An optimal stopping approach," IEEE Trans. Veh. Technol., vol.69, no.8, pp.10348–10361, 2020.
[16] R. Rezaei, M. Movahednasab, N. Omidvar, and M.R. Pakravan, "Stochastic power control policies for battery-operated wireless power transfer," IEEE 29th PIMRC, 2018.
[17] K.W. Choi, P.A. Rosyady, L. Ginting, A.A. Aziz, D. Setiawan, and D.I. Kim, "Theory and experiment for wireless-powered sensor networks: How to keep sensors alive," IEEE Trans. Wireless Commun., vol.17, no.1, pp.430–444, 2018.
[18] H. Dai, Y. Xu, G. Chen, W. Dou, C. Tian, X. Wu, and T. He, "ROSE: Robustly safe charging for wireless power transfer," IEEE Trans. Mobile Comput., vol.21, no.6, pp.2180–2197, 2022.
[19] A. Iqbal, Y. Kim, and T.-J. Lee, "Access mechanism in wireless powered communication networks with harvesting access point," IEEE Access, vol.6, pp.37556–37567, 2018.
[20] S. Bi, Y.J. Zhang, and R. Zhang, "Distributed scheduling in wireless powered communication network: Protocol design and performance analysis," 15th International Symposium on Modeling and Optimization in Mobile, Ad Hoc, and Wireless Networks (WiOpt), 2017.
[21] H. Choi and K. Lee, "Cooperative wireless power transfer for lifetime maximization in wireless multihop networks," IEEE Trans. Veh. Technol., vol.70, no.4, pp.3984–3989, 2021.
[22] E. Chen, M. Xia, and S. Aissa, "Coverage probability of hierarchical wireless networks with hybrid powering/relaying nodes," ISWCS 2018, 2018.
[23] Y. Zeng, H. Chen, and R. Zhang, "Bidirectional wireless information and power transfer with a helping relay," IEEE Commun. Lett., vol.20, no.5, pp.862–865, 2016.
[24] Z. Ding, I. Krikidis, B. Sharif, and H.V. Poor, "Wireless information and power transfer in cooperative networks with spatially random relays," IEEE Trans. Wireless Commun., vol.13, no.8, pp.4440–4453, 2014.
[25] A. Subhash and S. Kalyani, "Cooperative relaying in a SWIPT network: Asymptotic analysis using extreme value theory for non-identically distributed RVs," IEEE Trans. Commun., vol.69, no.7, pp.4360–4372, 2021.
[26] T. Le, K. Mayaram, and T. Fiez, "Efficient far-field radio frequency energy harvesting for passively powered sensor networks," IEEE J. Solid-State Circuits, vol.43, no.5, pp.1287–1302, 2008.
[27] B. Clerckx, "Wireless information and power transfer: Nonlinearity, waveform design, and rate-energy tradeoff," IEEE Trans. Signal Process., vol.66, no.4, pp.847–862, 2018.
[28] E. Boshkovska, D.W.K. Ng, N. Zlatanov, and R. Schober, "Practical non-linear energy harvesting model and resource allocation for SWIPT systems," IEEE Commun. Lett., vol.19, no.12, pp.2082–2085, 2015.
[29] G. Ma, J. Xu, Y. Zeng, and M.R.V. Moghadam, "A generic receiver architecture for MIMO wireless power transfer with nonlinear energy harvesting," IEEE Signal Process. Lett., vol.26, no.2, pp.312–316, 2019.
[30] S. Wang, M. Xia, K. Huang, and Y.-C. Wu, "Wirelessly powered two-way communication with nonlinear energy harvesting model: Rate regions under fixed and mobile relay," IEEE Trans. Wireless Commun., vol.16, no.12, pp.8190–8204, 2017.
[31] J. Kang, I. Kim, and D.I. Kim, "Joint Tx power allocation and Rx power splitting for SWIPT system with multiple nonlinear energy harvesting circuits," IEEE Wireless Commun. Lett., vol.8, no.1, pp.53–56, 2019.
[32] H. Saito, "Theoretical analysis of nonlinear energy harvesting from wireless mobile nodes," IEEE Wireless Commun. Lett., vol.10, no.9, pp.1914–1918, 2021.
[33] M. Haenggi, Stochastic Geometry for Wireless Networks, Cambridge University Press, 2013.
[34] B. Blaszczyszyn, M. Haenggi, P. Keeler, and S. Mukherjee, Stochastic Geometry Analysis of Cellular Networks, Cambridge University Press, 2018.
[35] H.H. Yang, T.Q.S. Quek, and H.V. Poor, "A unified framework for SINR analysis in Poisson networks with traffic dynamics," IEEE Trans. Commun., vol.69, no.1, pp.326–339, 2021.
[36] J.L. Folks and R.S. Chhikara, "The inverse Gaussian distribution and its statistical application — A review," Journal of the Royal Statistical Society. Series B (Methodological), vol.40, no.3, pp.263–289, 1978.
[37] M. Dominé, "Moments of the first-passage time of a wiener process with drift between two elastic barriers," Journal of Applied Probability, vol.32, no.4, pp.1007–1013, 1995.
[38] H. Wang and C. Yin, "Moments of the first passage time of one-dimensional diffusion with two-sided barriers," Statistics & Probability Letters, vol.78, no.18, pp.3373–3380, 2008.
[39] http://www9.plala.or.jp/hslab/supplement.html

Hiroshi Saito received a B.E. degree in Mathematical Engineering in 1981, an M.E. degree in Control Engineering in 1983, and a Dr.Eng. in Teletraffic Engineering in 1992 from the University of Tokyo. He joined NTT in 1983. Since 2018, he has been a professor at the University of Tokyo. Currently, he is an emeritus professor at the University of Tokyo and a specially-appointed professor at Jissen Women's University. He received the Young Engineer Award of the IEICE in 1990, the Telecommunication Advancement Institute Award in 1995 and 2010, the excellent papers award of the Operations Research Society of Japan (ORSJ) in 1998, the ACM MSWiM conference best paper award in 2016, the Arne Jensen Lifetime Achievement Award in 2020, and the IEICE Distinguished Achievement and Contributions Award in 2023. He has served as an editor and a guest editor of technical journals such as Performance Evaluation, Computer Networks, IEEE Journal of Selected Areas in Communications, and IEICE Trans. Communications; the organizing committee chairman and program committee chairman of several international conferences; a TPC member of more than 40 international conferences; and the director of the Journal and Transactions of IEICE. Dr. Saito is a fellow of IEEE, IEICE, and ORSJ and a member of IFIP WG 7.3. His research interests include traffic technologies of communications systems, network architecture, and applied mathematics in communications systems.